Stacking stability of MoS_2 bilayer: An *ab initio* study*

Tao Peng(陶 鹏), Guo Huai-Hong(郭怀红), Yang Teng(杨 腾)†, and Zhang Zhi-Dong(张志东)

Shenyang National Laboratory for Materials Science, Institute of Metal Research, Chinese Academy of Sciences, Shenyang 110016, *China*

(Received 25 March 2014; revised manuscript received 28 April 2014; published online 10 August 2014)

The study of the stacking stability of bilayer MoS_2 is essential since a bilayer has exhibited advantages over single layer MoS_2 in many aspects for nanoelectronic applications. We explored the relative stability, optimal sliding path between different stacking orders of bilayer MoS_2, and (especially) the effect of inter-layer stress, by combining first-principles density functional total energy calculations and the climbing-image nudge-elastic-band (CI-NEB) method. Among five typical stacking orders, which can be categorized into two kinds (I: *AA*, *AB* and II: AA', AB', $A'B$), we found that stacking orders with Mo and S superposing from both layers, such as AA' and *AB*, is more stable than the others. With smaller computational efforts than potential energy profile searching, we can study the effect of inter-layer stress on the stacking stability. Under isobaric condition, the sliding barrier increases by a few eV/(uc·GPa) from AA' to AB', compared to 0.1 eV/(uc·GPa) from *AB* to [*AB*]. Moreover, we found that interlayer compressive stress can help enhance the transport properties of AA'. This study can help understand why inter-layer stress by dielectric gating materials can be an effective means to improving MoS_2 on nanoelectronic applications.

Keywords: MoS_2, stacking order, climbing-image nudge-elastic band, isobaric sliding

PACS: 68.35.–p, 61.30.Hn, 68.65.Ac, 62.50.–p **DOI:** 10.1088/1674-1056/23/10/106801

1. Introduction

Two-dimensional crystals, especially graphene,[1] have been attracting increasing attention due to their demonstrated potential in nanoelectronic applications.[2] Unfortunately, the lack of a band gap leaves graphene with a very low on/off ratio[3] and the difficulty of tuning electronic structure in graphene hinders the immediate application in nanoelectronic devices. In this respect, transition metal dichalcogenides[1,4] (typically MoS_2), which preserve some good aspects of graphene, show their advantages over graphene in nanoelectronic devices,[5] such as its band gap tunability,[6–8] high on/off ratio[9] (up to 10^8), high intrinsic carrier mobility,[10] and low resistance contact.[11–13]

Compared to single layer, bilayer MoS_2 shows a pronounced improvement on applicable properties.[14] With a smaller band gap, bilayer can have a more observable field-induced effect.[15] A much improved mobility has also been observed in bilayer.[16] Moreover, with inversion symmetry preserved in the bilayer, MoS_2, with tunable Berry curvature and polarizability by an electric field, renders itself a better candidate for realizing valleytronic applications.[17] Few-layer MoS_2 has also been demonstrated experimentally to be more suitable than single-layer MoS_2 for applications in ambient conditions.[18]

The stacking structure or stacking order for few-layer MoS_2 including bilayer is obviously essential for determining the subsequent electronic properties. To quantify the relative stability of different stacking orders, Liang *et al.*[19] calculated the potential profile for sliding between two MoS_2 (001) surfaces, Blumberg *et al.*[20] determined the sliding potential of 2H–MoS_2 based on the registry index method. Their studies on bulk form have contributed greatly to the understanding of bilayer MoS_2 but were only limited on stacking orders, such as AA'. Among the studies on bilayer MoS_2, Liu *et al.*[21] obtained the relative stability of five typical stacking orders (*AA*, *AB*, AA', AB', and $A'B$ as defined later) from both local density approximation (LDA) and PBE + D calculations, He *et al.*[21] made a comparative study on the relative stability among the same five stacking orders from different van der Waals corrections, and also the stacking effect on the optical and electronic properties. They all obtained the most stable stacking geometry of AA', which of course has an instructive significance for applications. However, they did not calculate the sliding barriers between stacking orders, which nevertheless is quite an important part of evaluating stacking stability. Moreover, electrolyte dielectrics (i.e., HfO_2,[10] ionic liquid[11]) have been demonstrated experimentally as essential in improving device efficiency of MoS_2-based transistors. Theoretical studies show that these dielectric gatings may impose in-plane stress on MoS_2, therefore giving rise to an improved mobility.[22] However, interlayer stress effect will also be anticipated for a few-layer MoS_2, but how it influences both stacking stability and the corresponding electronic properties has not been theoretically touched upon.

In this study, we explored the relative stability, optimal sliding path between stacking orders, and effect of inter-

*Project supported by the National Natural Science Foundation of China (Grant Nos. 11004201 and 50831006) and the National Basic Research Program of China (Grant No. 2012CB933103). Yang Teng acknowledges the IMR SYNL-Young Merit Scholars and T.S. Kê Research Grant for support.

†Corresponding author. E-mail: yangteng@imr.ac.cn

© 2014 Chinese Physical Society and IOP Publishing Ltd

layer stress on stacking stability and the electronic properties of MoS_2 bilayer by combining first-principles density functional total energy calculations and the climbing-image nudge-elastic-band (CI-NEB) method. Our results suggest that an interlayer stress acts as an applicable means to improving both the stacking stability and the electronic mobility of bilayer MoS_2 for long-term applications on nanoelectronics.

2. Methods

Our calculation was based upon density functional theory (DFT) and projector augmented wave (PAW) pseudopotential method implemented in the Vienna *ab initio* Simulation Package (VASP).[23] The exchange–correlation potential was treated by the generalized gradient approximation (GGA) and the Perdew–Burke–Ernzerhof (PBE).[24] Van der Waals (VdW) interaction between the layers was calculated by using Grimme's DFT-D2 correction to the PBE functional.[25] A vacuum spacing of 30 Å was used to avoid inter-cell interaction. Considering the weak interlayer interaction in the order of meV, we set the kinetic cutoff energy to 650 eV and used $15 \times 15 \times 1$ k mesh for whole Brillouin zone to obtain total energy convergence better than 1 meV/atom. The interatomic force is minimized to be less than 0.005 eV/Å for structural optimization. Sliding energy barriers were evaluated using the CI-NEB method,[26,27] with nine intermediate images along each hypothetical sliding path between two stacking orders. Climbing images were added to estimate more accurately the height of the barriers. The force minimization for each image is also set to be less than 0.005 eV/Å. Compared to searching potential energy profile,[28] our combined study based on density functional theory and CI-NEB method costs much less in terms of computational effort.

3. Results and discussion

Five representative stacking orders (AA, AB, AA', AB', and $A'B$), which can almost exhaust all conceivable stacking configurations of bilayer MoS_2,[14,21] are shown in Fig. 1(a). The nomenclature of these five stacking orders can be referred to Ref. [11]. AA has the same atoms on both top and bottom layers, while AA' refers to Mo(S) of the top layer right above S(Mo) of the bottom layer. By shifting from AA (AA') along armchair direction to have one atom of top layer locates on top of the hexagon center of the bottom layer, we can obtain AB (AB' or $A'B$). Of course, the shifted stacking orders have superposition of atoms on both layers from the top view, for example, AB has the Mo–S superposition, AB' has the Mo–Mo, and $A'B$ has the S–S superposition. In terms of the existence or not of the inversion symmetry, all of these stacking orders having similar rotational symmetry can be categorized into two types: type I including the AA and AB without the inversion symmetry, and type II with the inversion symmetry, including AA', AB', and $A'B$. The stacking orders in each type can be switched to each other by a translational shift between the two sublayers, but an interlayer twisting is inevitable to switch between two types. Since interlayer twisting is much more complicated and costs much more energy than interlayer sliding, here we will not consider inter-type transition.

To explore the stacking stability of bilayer MoS_2, we calculated the formation energies E_{form} as a function of interlayer distance h in Fig. 1(b). The formation energy E_{form} is defined as the total energy difference per atom between bilayer and the two constituent single monolayers are well separated ($E_{\text{form}} = E_{\text{bilayer}} - 2E_{\text{monolayer}}$). Similar trends are found

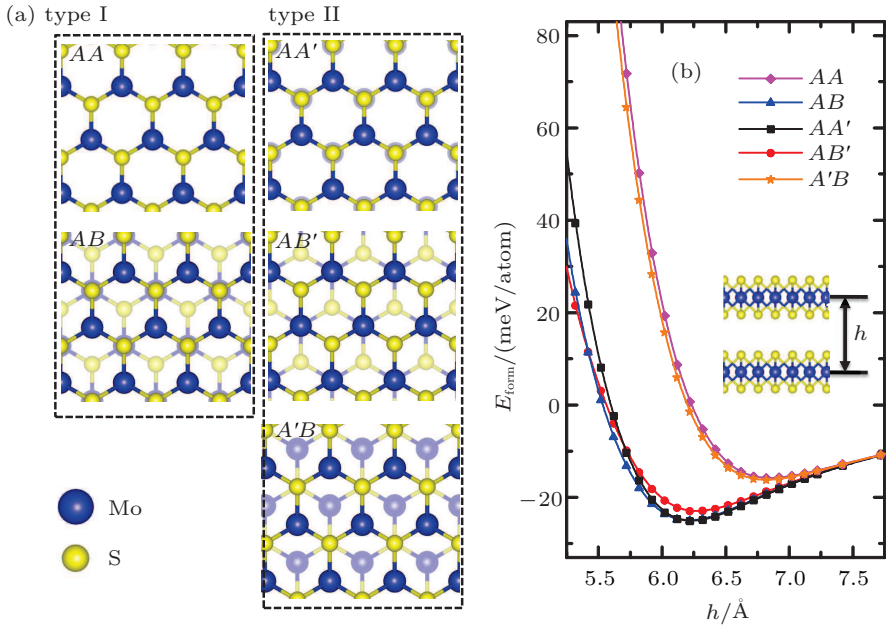


Fig. 1. (color online) (a) Stacking orders AA, AB, AA', AB', and $A'B$ categorized into two types. Type I: AA and AB, type II: AA', $A'B$, and AB'. (b) The formation energy (E_{form}) of five stacking orders as a function of inter-layer distance (h). Stacking orders AA and $A'B$ are the least stable among all orders.

among three stacking orders of AA', AB, and AB' and also between AA and $A'B$ in terms of the interlayer distance h_0 and formation energy in equilibrium. From Table 1, the h_0 and E_{form} for AA', AB, and AB' are around 6.25 Å and lower than −25.1 meV/atom, respectively, in contrast to 6.80 Å and −15.8 meV/atom for both AA and $A'B$, revealing that AA', AB, and AB' are much more stable than AA and $A'B$. Among the three relatively stable geometries of AA', AB, and AB', AA' and AB are more stable than AB'. Interlayer Coulomb interaction may play an important role in distinguishing the stability between the stacking orders. For example, the less instability of both AA and $A'B$ may be comprehended by a strong Coulomb repulsion between the two nearest sulfur atoms from two sublayers, while interlayer Coulomb attraction makes both AA' and AB more stable than AB'. It is worth noting that the stability hierarchy of stacking orders and interlayer distance from our calculations agree fairly quantitatively with that obtained by other vdW corrections.[14,21]

Table 1. The formation energy and corresponding interlayer distance h_0 at equilibrium for each stacking order.

Stacking order	AA'	AB	AB'	AA	$A'B$
h_0/Å	6.21	6.21	6.28	6.81	6.78
E_{form}/(meV/atom)	–25.13	–25.04	–22.98	–15.83	–16.04

What is more interesting in Fig. 1(b) is the swap of relative stability among AA', AB' and AB along with the decreasing h. All of the stacking orders converge naturally to one single curve if the interlayer spacing h is large enough, where stacking order does not affect formation energy. Since h is reduced to the equilibrium position, AB' becomes relatively unstable compared to AA' and AB due to the aforementioned different Coulomb interactions. Once the interlayer distance is further reduced, a stability difference between AA' and AB appears. AA' becomes relatively unstable than AB and even than AB', suggesting that the electrostatic Coulomb attraction alone cannot account for the relative stability among them. AB', which is the least stable among the three conformations in equilibrium, becomes the most stable one as h goes below 5.40 Å. This stability swap suggests the effect on the stacking stability of interlayer compressive stress. In the meantime, we have noticed that not only the formation energy but also the sliding barrier between stacking orders are important to determine the stacking stability as a whole. It is, therefore, necessary to uncover possible sliding pathway and pin down the value of barriers.

We expect that the optimal sliding route will pass through these stacking orders since formation energy local minimum (or maximum) usually occurs in those high-symmetry stacking structures. Indeed, as shown in Fig. 2, we obtained the optimal pathway by connecting all possible stacking conformations, similar to those found in a similar BN system but based on potential profile searching[28,29] and with higher computational cost. During our CI-NEB calculations, these stacking structures serve as both initial state and final state in the sliding process.

We start with the type I and are only concerned with the sliding between the stacking order AB and AA. A hypothesized route is schematized in Fig. 2(a), in which AB and $[AB]$ simply have a mirror symmetry with respect to each other and should be identical. The optimized pathway obtained from CI-NEB calculation agrees with the hypothesized route and the energy profile along this route obtained is shown in Fig. 2(b). As expected, AA and AB locate at an energy maximum and minimum in the sliding pathway, respectively. AA has an energy of 9.1 meV/atom higher than AB and will spontaneously slide away towards AB stacking. Between AB and $[AB]$, a sliding barrier is found to be 2.4 meV/atom and is much smaller than the energy cost through AA. This indicates an optimal sliding pathway along a zigzag line connecting the AB and $[AB]$ (namely, $AB \rightarrow [AB] \rightarrow AB$), as illustrated in Fig. 2(c). Interestingly, we set up another possible sliding route directly between two nearest AB (black dashed line in the left panel of Fig. 2(c)), but still a zigzag route (solid red line) is desired by the CI-NEB calculation. From Fig. 2(c), we also found that the interlayer distance h goes up and down in lines with the energy profile along the optimal pathway.

The sliding pathway for the type II is expected to be more complicated than that for type I, obviously due to more choices of the sliding way. As discussed before, we selected a straight route covering all three stacking orders, as illustrated in Fig. 2(d). Starting from AA', a complete cycle includes two intermediate AB' and $A'B$. From CI-NEB calculations, as shown in Fig. 2(e), we found that AA' lies at a global energy minimum and AB' at a local energy minimum, but $A'B$ is quite unstable at an energy maximum and should be avoided during a sliding process. A similar zigzag optimal pathway is anticipated, such as $AA' \rightarrow AB' \rightarrow AA'$, and a direct route between AA' and AA' is also overruled, as schematized by solid red line other than black dashed line in the left panel of Fig. 2(f). The energy barrier of 3.2 meV/atom obtained is higher than that in the type I, which suggests a higher stacking stability of the type II. It is worth pointing out that we have so far only considered an ambient situation without any stress applied.

To explore the interlayer compression effect on sliding behavior and stacking stability of MoS_2 bilayer, we calculated energy along the optimal sliding pathway as a function of interlayer distance. Here we used Δd to represent the horizontal deviation from AB along $AB \rightarrow [AB]$ path or from AA' along $AA' \rightarrow AB'$ path, which is shown in Figs. 3(a) and 3(d), and chose $\Delta h (= h - h_0)$ for the change of interlayer distance h with respect to h_0 of the most stable geometry (i.e., of AB or of AA'). Promisingly, we found that Δd obtained from CI-NEB calculations always follows the horizontal straight route for both $AB \rightarrow [AB]$ and $AA' \rightarrow AB'$ paths under various interlayer compressions. At each point (Δh, Δd), we obtained energy

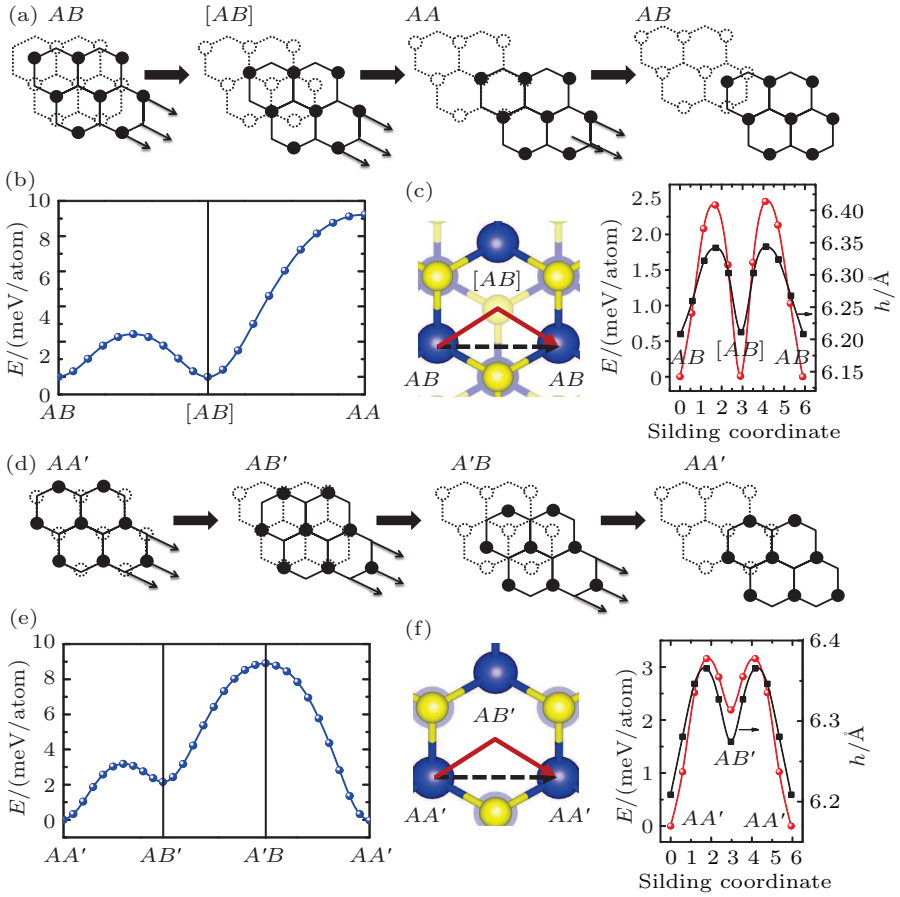


Fig. 2. (color online) (a)–(c) Sliding pathway between *AB* and *AA*. (a) Schematics of relative sliding motion. Filled (empty) circles represent Mo atoms at top (bottom) layer, the remaining unmarked are S atoms. (b) Energy profile along the sliding coordinate from one order to another, obtained from the CI-NEB method. (c) Left panel: Schematics showing that, starting from a simple hypothesized straight pathway from *AB* to *AB* (as indicated by black dashed line), CI-NEB searching finds an optimal zigzag sliding pathway (as indicated by red solid line). Right panel: Energy profile and optimized inter-layer distance h along the optimal pathway during a complete sliding cycle. (d)–(f) Sliding pathway between AA', AB', and $A'B$ stacking orders. (d) Schematics of relative sliding along a straight line connecting all three stacking orders. (e) Energy profile along the sliding coordinate from one stacking to another. (f) Energy profile and optimized inter-layer distance h along the optimal pathway for one complete sliding cycle. A zigzag sliding route is also found.

change and interlayer stress P and, therefore, can make a three-dimensional plot as shown in Figs. 3(b) and 3(e). Along with increasing Δh, both sliding energy barriers and interlayer stress P (red lines projected in the horizontal plane) increase. By sliding along the iso-Δh line, the variation of interlayer stress also increases with Δh, especially along the $AA' \rightarrow AB'$ pathway. An interlayer compression of up to 1.0 Å of Δh induces approximate 2.8 GPa of interlayer stress for *AB* geometry, 3.5 GPa for AA', and 1.7 GPa for AB', suggesting different elasticities among *AB*, AA', and AB' stacking orders.

Practically, isobaric sliding process is more straightforward to observe the compression effect on the stacking stability. Based on the three-dimensional plot in Figs. 3(b) and 3(e), we derived contour plots of both isobaric and iso-energy lines with respect to Δd and Δh in Figs. 3(c) and 3(f). The energy interval is set to be 0.03 eV/uc (uc: unit cell, or per 6 atoms) and stress interval 0.30 GPa. Similar messages in Figs. 3(c) and 3(f) can be obtained, as in Figs. 3(b) and 3(e), such as Δd dependence of energy and stress along each iso-line of h. Meanwhile, with Δh decreasing from 0.0 to -1.0 at a fixed Δd, stacking energy increases with elevating stress. Additionally, we can observe in Figs. 3(c) and 3(f) how both energy (and sliding barrier) and interlayer distance h vary along isobaric lines. The sliding barrier at a given stress can basically be extracted from a simple counting of number of iso-energy lines that the iso-baric line crosses. The bigger the number of crossings are, the higher the sliding barrier will be. Unusually, we found in Fig. 3(c) that the sliding barrier initially increases slightly with compressive stress P, and then saturates once P is above some threshold values. This suggests that lubricant properties of *AB*-stacking MoS_2 are insensitive to the vertical compression. However, compared to the $AB \rightarrow [AB]$ pathway, $AA' \rightarrow AB'$ shows a more drastic character in that the sliding barrier increases all the way with increasing compressive stress, indicating interlayer stress as a useful means for improving stacking stability.

The positive effect of interlayer stress on the AA' stacking is reflected not only on improving the stacking stability of AA' with respect to other stacking orders but also on the enhancement of transport properties, such as the reduction of both band gap and carrier effective mass, which contribute to the enhanced quality of nanoelectronic devices. From Fig. 4(a), along with the elevating stress, band gap from Γ

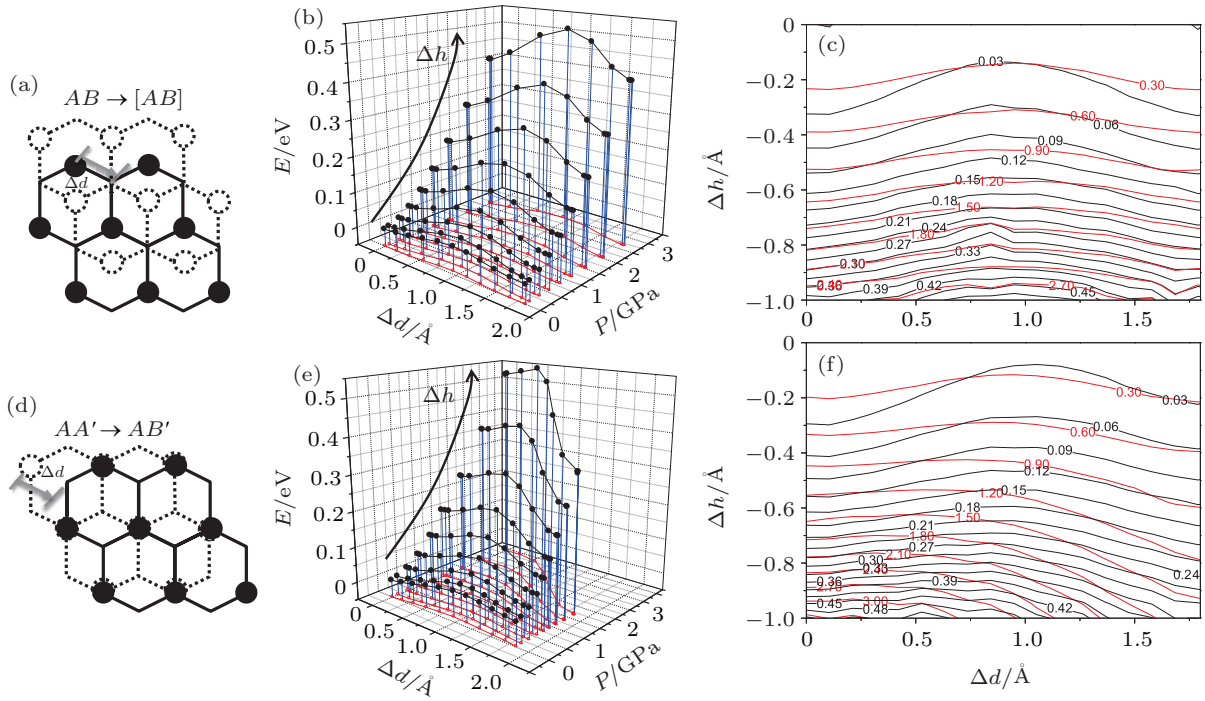


Fig. 3. (color online) Interlayer compression effect on the optimal sliding pathway. Panels (a)–(c) show the sliding from *AB* to [*AB*], panels (d)–(f) show that from *AA*′ to *AB*′. Panels (b) and (e) are three-dimensional plots of energy as a function of sliding distance Δd, compression Δh, and compression stress P. Δh (with respect to the equilibrium h_0 for geometry *AB* and *AA*′) changes by an interval value of 0.125 Å. To study a practical isobaric situation, contour plots in panels (c) and (f) are given to show the isolines of energy and compressive stress as a function of Δd and Δh. Red lines represent the isobaric pathway with stress unit of GPa while black ones the iso-energy lines with unit of eV. As pressure increases, the sliding barrier changes and affects solid lubricant efficiency.

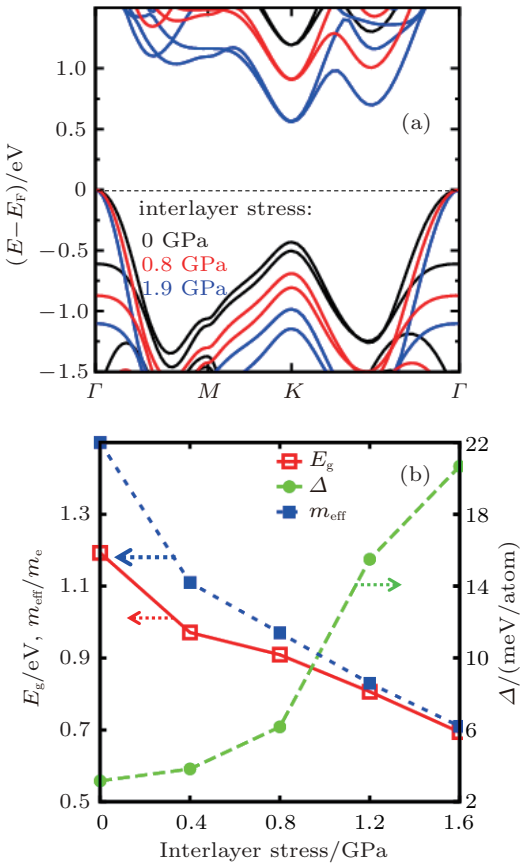


Fig. 4. (color online) Interlayer stress effect on band gap E_g, effective mass m_{eff}, and sliding barrier Δ for MoS_2 *AA*′ stacking structure. Stress reduces E_g and m_{eff} of carriers on the top of valence band, while it increases the stacking stability by enhancing Δ.

to *K* decreases, whereas band curvature on the top of the valence band at Γ increases, which is indicative of a decreasing effective mass m_{eff} of carrier and therefore a strain-induced mobility enhancement.[30] These changes are also quantified in Fig. 4(b). The m_{eff} of carrier decreases by 0.33 m_e/GPa and goes even smaller than the electron mass for the stress above 0.8 GPa, where the sliding barrier to deviate from *AA*′ stacking increases abruptly with stress.

4. Conclusion

We explored the relatively stable, optimal sliding path between different stacking orders of bilayer MoS_2, and also the effect of interlayer stress, by combining first-principles density functional calculations with the climbing-image nudge-elastic-band (CI-NEB) method. For five typical stacking orders, which can be categorized into two kinds (I: *AA*, *AB* and II: *AA*′, *AB*′, *A*′*B*), the long-range electrostatic interaction is more essential than the dispersion force in determining the relative stability among them, and stacking orders with Mo and S superposing from both layers, such as *AA*′ and *AB*, is more stable than the others. The CI-NEB method helps save computational efforts and facilitates the study of the interlayer stress effect on stacking stability. In contrast to the modest effect on the type I, stress changes the sliding barrier and relative stability more substantially between the stacking orders of type II. Under isobaric conditions, the sliding barrier increases by a few eV/(uc·GPa) from *AA*′ to *AB*′, in contrast to

0.1 eV/(uc·GPa) from AB to $[AB]$. Moreover, we found that interlayer compressive stress can help enhance the transport properties of AA'. This study can help us to understand why the inter-layer stress induced by dielectric gating materials can be an effective means to improving MoS_2 on nanoelectronic applications.

References

[1] Novoselov K S, Jiang D, Schedin F, Booth T J, Khotkevich V V, Morozov S V and Geim A K 2005 *Proc. Natl. Acad. Sci. USA* **102** 10451
[2] Westervelt R M 2008 *Science* **320** 324
[3] Xia F, Farmer D B, Lin Y M and Avouris P 2010 *Nano Lett.* **10** 715
[4] Coleman J N, Lotya M, O'neill A, Bergin S D, King P J, Khan U, Young K, Gaucher A, De S, Smith R J, Shvets I V, Arora S K, Stanton G, Kim H Y, Lee K, Kim G T, Duesberg G S, Hallam T, Boland J J, Wang J J, Donegan J F, Grunlan J C, Moriarty G, Shmeliov A, Nicholls R J, Perkins J M, Grieveson E M, Theuwissen K, McComd D W, Nellist P D and Nicolosi V 2011 *Science* **331** 568
[5] Wang H, Yu L, Lee Y H, Shi Y, Hsu A, Chin M L, Li L J, Dubey M, Kong J and Palacios T 2012 *Nano Lett.* **12** 4674
[6] Conley H J, Wang B, Ziegler J I, Haglund R F, Pantelides S T and Bolotin K I 2013 *Nano Lett.* **13** 3626
[7] Mak K F, Lee C, Hone J, Shan J and Heinz T F 2010 *Phys. Rev. Lett.* **105** 136805
[8] Kumar A and Ahluwalia P 2012 *Eur. Phys. J. B* **85** 186
[9] Yoon Y, Ganapathi K and Salahuddin S 2011 *Nano Lett.* **11** 3768
[10] Radisavljevic B, Radenovic A, Brivio J, Giacometti V and Kis A 2011 *Nat. Nanotechnol.* **6** 147
[11] Perera M M, Lin M W, Chuang H J, Chamlagain B P, Wang C, Tan X, Cheng M M C, Tománek D and Zhou Z 2013 *ACS Nano* **7** 4449
[12] Das S, Chen H Y, Penumatcha A V and Appenzeller J 2013 *Nano Lett.* **13** 100
[13] Popov I, Seifert G and Tománek D 2012 *Phys. Rev. Lett.* **108** 156802
[14] He J, Hummer K and Franchini C 2014 *Phys. Rev. B* **89** 075409
[15] Ramasubramaniam A, Naveh D and Towe E 2011 *Phys. Rev. B* **84** 205325
[16] Baugher B W H, Churchill H O H, Yang Y and Jarillo-Herrero P 2013 *Nano Lett.* **13** 4212
[17] Wu S, Ross J S, Liu G B, Aivazian G, Jones A, Fei Z, Zhu W, Xiao D, Yao W, Cobden D and Xu X 2013 *Nat. Phys.* **9** 149
[18] Qiu H, Pan L, Yao Z, Li J, Shi Y and Wang X 2012 *Appl. Phys. Lett.* **100** 123104
[19] Liang T, Swayer W G, Perry S S, Sinnott S B and Phillpot S R 2008 *Phys. Rev. B* **77** 104105
[20] Blumberg A, Keshet U, Zaltsman I and Hod O 2012 *J. Phys. Chem. Lett.* **3** 1936
[21] Liu Q, Li L, Li Y, Gao Z, Chen Z and Lu J 2012 *J. Phys. Chem. C* **116** 21556
[22] Yun W S, Han S W, Hong S C, Kim I G and Lee J D 2012 *Phys. Rev. B* **85** 033305
[23] Kresse G and Furthmüller J 1996 *Phys. Rev. B* **54** 11169
[24] Perdew J P, Burke K and Ernzerhof M 1996 *Phys. Rev. Lett.* **77** 3865
[25] Grimme S 2006 *J. Comput. Chem.* **27** 1787
[26] Henkelman G, Uberuaga B P and Jónsson H 2000 *J. Chem. Phys.* **113** 9901
[27] Henkelman G and Jónsson H 2000 *J. Chem. Phys.* **113** 9978
[28] Constantinescu G, Kuc A and Heine T 2013 *Phys. Rev. Lett.* **111** 036104
[29] Marom N, Bernstein J, Garel J, Tkatchenko A, Joselevich E, Kronik L and Hod O 2010 *Phys. Rev. Lett.* **105** 046801
[30] Guo H H, Yang T, Tao P, Wang Y and Zhang Z D 2013 *J. Appl. Phys.* **113** 013709